Aerodynamic Performance Enhancement Using Active Flow Control on DU96-W-180 Wind Turbine Airfoil

Halawa, Amr M.
Interdisciplinary Graduate School of Engineering Sciences, Kyushu University | Department of Aerospace Engineering, Faculty of Engineering, Cairo University

Elhadidi, Basman
School of Mechanical & Aerospace Engineering, Nanyang Technological University

Yoshida, Shigeo
Research Institute for Applied Mechanics, Kyushu University

https://doi.org/10.5109/1929723

出版情報：Evergreen. 5 (1), pp.16-24, 2018-03. Green Asia Education Center
バージョン：

Aerodynamic Performance Enhancement Using Active Flow Control on DU96-W-180 Wind Turbine Airfoil

Amr M. Halawa[1,2,*], Basman Elhadidi[3], Shigeo Yoshida[4]

[1]Interdisciplinary Graduate School of Engineering Sciences, Kyushu University, Japan

[2]Department of Aerospace Engineering, Faculty of Engineering, Cairo University, Egypt

[3]School of Mechanical & Aerospace Engineering, Nanyang Technological University, Singapore

[4]Research Institute for Applied Mechanics, Kyushu University, Japan

*Author to whom correspondence should be addressed,
E-mail: amrhalawa@riam.kyushu-u.ac.jp

(Received January 10, 2018; accepted March 10, 2018).

In this work, the objective was to investigate the influence of Active Flow Control on the improvement of a DU96-W-180 airfoil aerodynamic performance. A numerical simulation was done for incompressible unsteady low Reynolds Number flow at high angle of attack. The innovative approach was the use of an "Active Slat" where the periodic blowing effect was achieved by periodically opening and closing the slat passage. The major benefit of this concept is being flexible to a desired operating condition. A new OpenFOAM® solver was developed from the existing *pisoFoam* solver to simulate the active slat flow control technique. To get the best aerodynamic performance, the active slat should operate at the domain dominant frequencies. A Fast Fourier Transform (FFT) was performed to achieve the optimum slat excitation frequency. These frequencies will help in controlling the inherent instabilities in the boundary layer and thus improving the aerodynamic performance. Finally, active flow control simulations were applied using different excitation. Using the optimum FFT excitation frequency ($\bar{f} = 0.68$ in the wake region) yields the best aerodynamic improvement of all tested frequencies. Improvements in lift coefficient were achieved up to 8%. Hence, the slatted airfoil is superior to the conventional clean configuration airfoil.

Keywords: Active Flow Control, Active Slat, CFD, FFT, OpenFOAM.

Nomenclature

Acronyms

AFC	:	Active Flow Control
CFD	:	Computational Fluid Dynamics
FFT	:	Fast Fourier Transform
MEMS	:	Micro-Electro-Mechanical-Systems
MLSM	:	Modified Linear Stochastic Measurement
PFC	:	Passive Flow Control
PISO	:	Pressure implicit with splitting of operator
POD	:	Proper Orthogonal Decomposition
ZNMF	:	Zero-net mass-flux

Greek Symbols

α	:	Angle of attack
Δ	:	Difference / Change operator
μ_{air}	:	Dynamic viscosity of air
ν_{air}	:	Kinematic viscosity of air
ρ_{air}	:	Density of air

Roman Symbols

c	:	Chord length
C_D	:	Drag coefficient
C_L	:	Lift coefficient
C_P	:	Pressure coefficient
f	:	ZNMF actuation frequency
$\bar{f}$	:	Non-dimensional frequency parameter
Re	:	Reynolds number
t	:	Time variable
$\bar{t}$	:	Non-dimensional time variable
U_∞	:	Free-stream velocity

1. Introduction

Flow control studies and its relevant applications had experienced great development in the past few decades. It is a fast growing multi-disciplinary scientific field aiming

at changing a natural state of flow to a more efficient state. Modern flow control methods are majorly applied to achieve drag reduction, lift enhancement, transition delay, separation postponement, mixing augmentation, flow-induced noise suppression, turbulence management ... etc[1-4]. Controlling the complex flow structures and achieving a mature understanding of their behavior and characteristics will surely have a noteworthy practical impact. The shapes and dimensions of any wings, blades, nozzles, diffusers, combustion chambers, ground/submerged vehicles, and so forth will be highly renovated. Moreover, new efficient designs could be achieved that allow for applications at higher speeds, range, and endurance yet with less fuel consumption. Furthermore, in case of wind turbine blades, the power production will be much maximized. Simply, any mechanical machinery related to the flow of fluids, whether externally or internally, will probably have a different looking and performance in the forthcoming decades[2-4]. There are so many successfully applied flow control applications starting from Passive Flow Control (PFC) actuators to the modern Micro-Electro-Mechanical-Systems (MEMS). A good quantitative comparison was performed by Barlas and Kuik[5] for the improved aerodynamic performance of wind turbines flow using different actuators. The feasibility of these active flow control AFC actuators was discussed where Microtabs showed high lift performance in addition to their simplicity and low power consumption. Morphing (camber control) method was highly efficient for increasing lift but difficult from the perspective of structure implementation until new techniques and smart materials could be used. One of the promising flow control actuators was the trailing edge flap that showed high lift improvement while being simple with linear response. It was applied successfully in free shear flows by Cattafesta et al.[6] in 2001 as well as its application in flow-induced cavity oscillations by Mathew et al.[7] in 2006.

On the other hand, Active Twist showed remarkable flow control yet it was not efficient technique. It suffered heavy blades, high power consumption and elevated operational cost. The remaining boundary-layer-based flow control techniques (synthetic jets, suction/blowing, plasma, etc) showed enhanced lift for high angles of attack near stall, however insignificant effect at low angles of attack[8].

Furthermore, Zero-net mass-flux (ZNMF) actuators, frequently called synthetic jets, were successfully implemented in many applications in the flow control field as noted by Glezer and Amitay[9] in 2002 and also by Raju et al.[10] in 2005. The popularity of ZNMF actuators in many applications is because they do not need any external source of flow, aside from their ability to produce complex vortices using different transduction schemes. Recently, plasma actuators have acquired great reputation among researchers since they have rapid time response due to the absence of moving parts, along with their solid-state nature, and small weight[11]. It has been studied extensively by Moreau[12] in 2007 and Corke et al.[13] in 2010.

Moreover, slats are aerodynamic surfaces attached to the wing leading edge allowing the passage of the air from below its lower surface to the upper surface. They provide some kind of blowing control into the boundary layer by a fresh jet of air that has higher energy than that of the boundary layer as shown in Fig. 1. That fresh jet of air adds an extra flow momentum to the upper surface flow that enhances the mixing of flow in the boundary layer. Consequently, a thicker boundary layer profile is achieved that can withstande high adverse pressure gradients and maintain attached flow (delaying separation) for longer distances. As a result, improved aerodynamic efficiency and operation at reduced stall speeds and higher angles of attack could be easily achieved. It also reduces the high concentrated pressure near the leading edge by changing the camber of the nose[14-15].

(a) (b)

Fig. 1: Flow over: (a) Clean configuration airfoil. (b) Slatted airfoil.

Based on the novel study of Elhadidi et al.[16] in 2015, an active slat on DU96-W-180 airfoil was implemented as in Fig. 2a where the blowing effect was achieved by the means of a simply designed actuator which is a vane rotating inside a stationary slat. The main benefit is its flexibility according to the specified operating condition. It might be fully closed, open or even actuated actively to induce the flow. Their experimental results indicated success in achieving a reduced mean pressure and an increased mean velocity on the upper surface of the airfoil at all the studied positive angles of attack, thus higher resultant lift as in Fig. 2b.

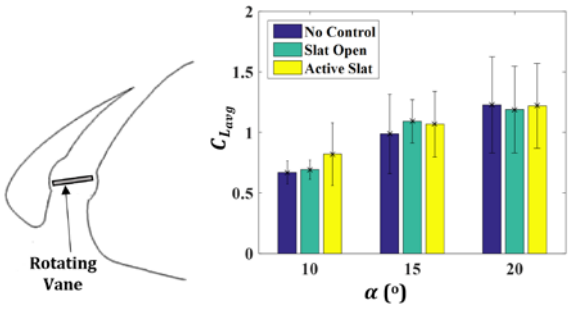

(a) (b)

Fig. 2: The novel active slat study: (a) Active slat actuator modeling. (b) Comparison between the lift coefficient numerical results for different cases[16].

In addition, Soltan[15] in 2015 applied the same active slat concept to a NACA 4418 at Reynolds Number, *Re* = 40,000 where improved lift and drag values were

achieved. A similar technique to the latter one was applied in this paper with more advanced approaches like the Fast Fourier Transform Analysis and Reduced Order modeling.

2. Methodology

In this section, a numerical simulation was done for an incompressible, unsteady airflow over a DU96-W-180 airfoil using OpenFOAM v2.3.0[19]. Firstly, the case description and assumptions are introduced then followed by the resulting governing equations. Next, the mesh description around the airfoil is shown along with the corresponding OpenFOAM boundary conditions. Next, the resulting governing equations are shown. Moreover, a sensitivity study was undertaken to ensure convergence followed by frequency analysis using Fast Fourier Transform (FFT) technique. Finally, the active flow control OpenFOAM solver was introduced.

2.1 Case description

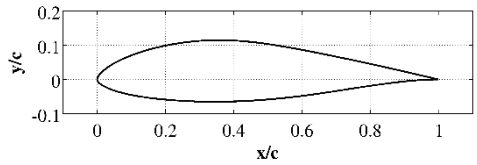

Fig. 3: Profile of DU96-W-180 airfoil.

In these simulations, the flow is assumed two-dimensional, laminar, incompressible, and low *Re* flow. The flow simulations around DU96-W-180 airfoil whose profile is shown in Fig. 3 are done with the geometrical and airflow parameters summarized in Table 1.

Table 1: A list for the basic flow and airfoil parameters.

Parameter	Value	Unit
α	10	[^{o}]
Re	5×10^4	[−]
μ_{air}	1.789×10^{-5}	$[kg/(m.s)]$
ρ_{air}	1.225	$[kg/m^3]$
ν_{air}	1.461×10^{-5}	$[m^2/s]$

2.2 Governing equations

In the light of the previous assumptions, the required Navier-Stokes equations to be solved through CFD are simplified to the following incompressible continuity and momentum equations:

$$\nabla \cdot \boldsymbol{U} = 0 \tag{1}$$

$$\frac{\partial \boldsymbol{U}}{\partial t} + \nabla \cdot (\boldsymbol{U}\,\boldsymbol{U}) - \nabla \cdot (\nu \nabla \boldsymbol{U}) = -\frac{\nabla \boldsymbol{p}}{\rho} \tag{2}$$

where, $\boldsymbol{U}$ is the velocity vector, while $\boldsymbol{p}$ is the pressure field. These equations were implemented within OpenFOAM's *pisoFoam* solver using the PISO algorithm.

2.3 Mesh description and case setup

A 2D dense mesh was constructed around a DU96-W-180 airfoil using ANSYS ICEM CFD as shown in Fig. 4. The mesh is an unstructured C-grid extending from 5 chords upstream to 10 chords downstream. It is split into 8,220 quad-elements and 139,989 tri-elements with stats as follows [points: 157,510, faces: 523,382, internal faces: 225,883, cells: 148,209, faces per cell: 5.05546]. Fig. 5a and Fig. 5b show a special mesh refinement that was done to fit the boundary layer near the airfoil wall.

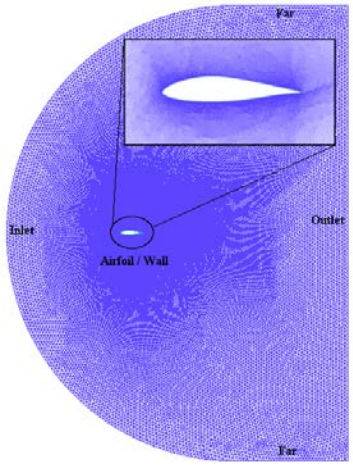

Fig. 4: The constructed mesh around DU96-W-180 airfoil with the boundary conditions patches.

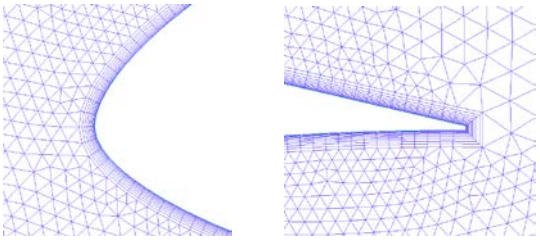

(a) The leading edge mesh. (b) The trailing edge mesh.

Fig. 5: A closer view on the mesh cells around DU96-W-180 airfoil.

The boundary conditions of the problem are defined along 5 patches as shown in Fig. 4. The pressure is *zeroGradient* everywhere except for the outlet where its value is known to be atmospheric pressure. However, for the velocity, it is *fixedValue* and equal to the uniform freestream value at the inlet and the far boundaries, calculated for the outlet while for the wall boundary, it reduces to zero (due to no-slip condition). The chosen solver is *pisoFoam* which is used to solve incompressible unsteady flow by a PISO algorithm with a generic turbulence model option. For this problem case with low *Re*, the turbulence model is turned off to solve for laminar flow only. To ensure convergence, a sensitivity study was carried on. Three different probe locations (#3 near the

separation bubble, #2 near the shear layer, and #1 in the wake region) were chosen in the computational domain for this study as plotted in Fig. 6.

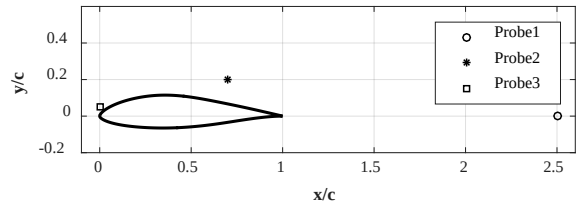

Fig. 6: The probes locations used for sensitivity studies.

Different time resolutions were tested for those probes. From Fig. 7a and Fig. 7b, it is clear that standard deviation values for both C_P and U are relatively small for all probes. Thus using 0.05 s time step will be efficient and yield time independent solution with acceptable error. Furthermore, since the mesh used in this paper is much denser than the one used by Soltan[15] and comparable to Elhadidi et al.[16] so a grid independence is guaranteed for this study.

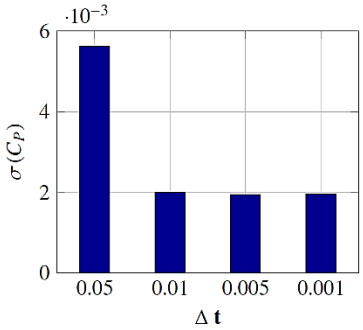

(a) Pressure coefficient standard deviation at different time steps.

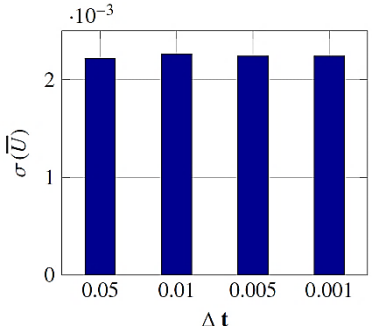

(b) Normalized velocity standard deviation at different time steps.

Fig. 7: Statistical analysis of the time sensitivity study at Probe #2.

2.4 Fast Fourier Transform (FFT)

To get the best aerodynamic performance, the active slat should operate at the domain dominant frequencies. An FFT frequency analysis was performed to achieve the optimum slat excitation frequency. These frequencies will help in controlling the inherent instabilities in the boundary layer and thus improving the flow properties. According to the study done by Raju et al.[17] three distinctive locations have the most dominant frequencies affecting the vortical structures in the flow, the separation wake, the shear layer, and the separation bubble regions. Thus, those three locations will be discussed as shown later in the results section.

2.5 Active flow control's OpenFOAM solver

A new solver was developed from the existing *pisoFoam* solver that was able to periodically excite the flow on the upper surface of the airfoil. That was achieved through modifying the pressure equation by adding a source term. To numerically simulate the effect of periodic opening and closing of the slat, a Darcy-Forcheimer porosity model was applied in the source term as in Eq. (3).

$$S = |sin(2\pi f \times t)| \times DarcyForchModelCoeff \quad (3)$$

Where, t is the simulation runtime, f is chosen from various frequencies including the dominant frequency resulted from FFT analysis, and *DarcyForchModelCoeff* [19] are defined as prescribed in OpenFOAM's *fvOptions* by Halawa[18, 23]. The main objective of this model is to change the density of a bulk of cells spanning the passage of the slat as shown in Fig. 8 (the cells enclosed by the orange rectangle). The density varies periodically (as a function of the running time) from a very high value (simulating a fully closed slat) back to the air density (simulating a fully open slat).

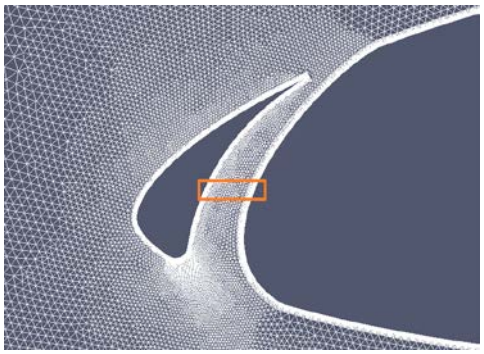

Fig. 8: Slat mesh and the cells responsible for AFC.

3. Results and discussions

3.1 Uncontrolled flow

In this section, simulations for both clean configuration airfoil and slatted airfoil will be shown. The computations were carried on till $\bar{t} = 47.45$ (130,000 time-step of 0.05 s) where $\bar{t}$ is non-dimensional time parameter defined as,

$$\bar{t} = \frac{t \times U_\infty}{c} \quad (4)$$

where U_∞ is the free stream velocity and c is the chord.

Firstly, the unslatted (clean configuration) airfoil case was simulated. The normalized velocity distribution for the computational domain is presented in Fig. 9 where the

unsteady Kármán vortex shedding is obvious after the trailing edge of the airfoil.

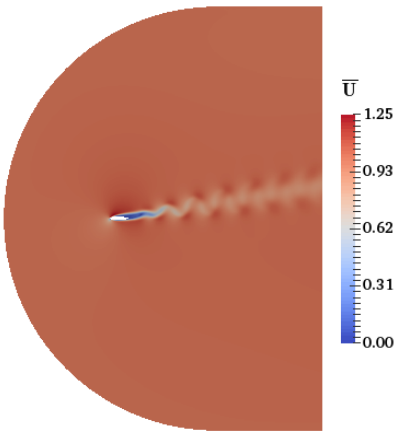

Fig. 9: The velocity distribution around the airfoil at $\bar{t} = 47.45$ showing the unsteady Kármán vortex shedding.

Next, the flow field is simulated for the case of uncontrolled slat. The results shown in Fig. 10a and Fig. 10b are for the velocity contours for the open slat case, where the source term is zero, and the closed slat case (exactly resembles the clean airfoil case), where the source term is nonzero and controlled by the Darcy Forchheimer Porosity Model in the OpenFOAM library, respectively.

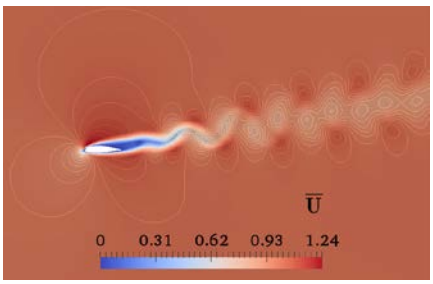

(a) Open-slatted airfoil case.

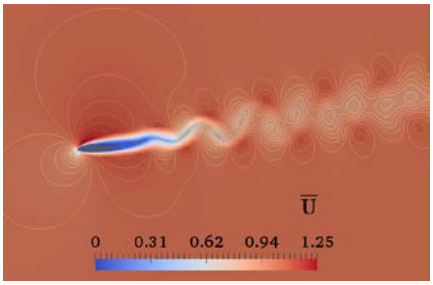

(b) Closed-slatted airfoil case.

Fig. 10: Velocity contours for the flow around the DU96-W-180 airfoil.

It is worthy to note that as shown from Fig. 10a and Fig. 10b, both the open and closed slat simulations showed similar trailing edge shedding, thus any application of reduced order modelling as the POD/MLSM methods on either of them is acceptable[18, 23] as verified with El-desouky's research[24] too.

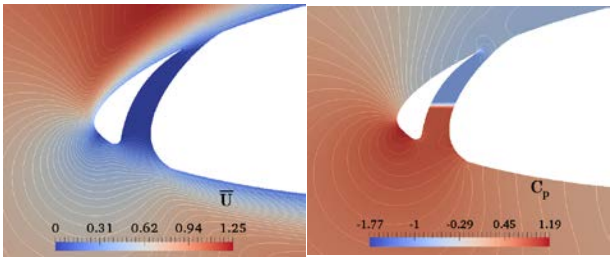

(a) (b)

Fig. 11: Close-up view on the flow variables contours for the flow around the closed-slatted DU96-W-180 airfoil. (a) Normalized velocity contours. (b) Pressure coefficient contours.

Furthermore, Fig. 11a and Fig. 11b show a close-up view for velocity and pressure contours of the case of the closed-slatted airfoil simulations, respectively. That is clearly showing the effect of the slat blockage on the velocity that is reduced to zero inside the slat that resembles the case of no-slat airfoil (clean configuration). On top of that, the accumulation of the flow in the lower portion of the slat led to a high-pressure zone as shown.

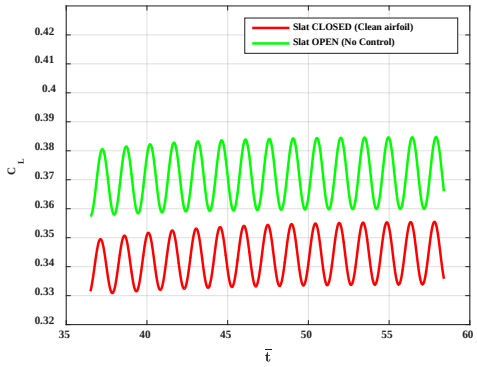

(a) Temporal variation of the Lift coefficient.

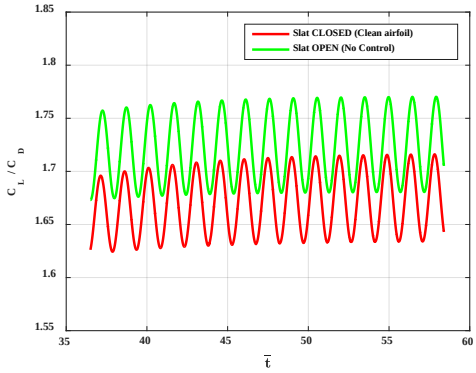

(b) Temporal variation of the Aerodynamic efficiency.

Fig. 12: Aerodynamic properties time variation for clean/slatted airfoil.

Moreover, a noticeable improvement in the aerodynamic properties was achieved due to the open slat as shown in the Fig. 12a and Fig. 12b. The lift coefficient was boosted by around 8% of its value when the slat was closed (clean configuration/ no-slat case). Furthermore, an improvement in aerodynamic efficiency was achieved by about 3.1%.

3.2 Fast Fourier Transform (FFT)

As shown in Fig. 13, three probe locations were chosen to match the three distinctive locations that were under investigation. The probe locations have coordinates as follows:
Probe #1 (Wake region): (x1, y1) = (17.537, 2.557)
Probe #2 (Shear Layer region): (x2, y2) = (4.115, 2.055)
Probe #3 (Separation Bubble region): (x3, y3) = (0.894, 0.744)

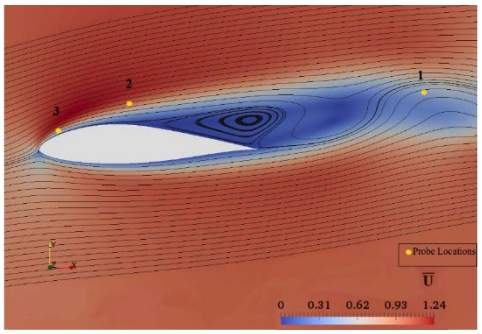

Fig. 13: The three probe locations used to study FFT.

Theses probe locations data were extracted and then a Fast Fourier Transform (FFT) routine was constructed and applied using 20 Hz sampling frequency to the normalized cross-stream velocity, $\overline{U}_y$, variation as shown in Fig. 14a to Fig. 14c where,

$$\overline{U}_y = \frac{U_y}{U_\infty} \tag{5}$$

In addition, the frequency value in the other regions of the mixing shear layer as in Fig. 14b, and the separation bubble as in Fig. 14c is so small (near zero) indicating very small vortical structures at these regions and thus insignificant impact on the overall domain dominant frequencies. Hence, actuating using the previously obtained dominant frequency should yield a better aerodynamic response and would save time in trial and error tests in the active control phase as discussed in the following section. As shown in Fig. 14a, the dominant frequency was found to be $\bar{f} = 0.68$ and obviously appeared in the wake region which has the most energy content by nature where,

$$\bar{f} = \frac{f \times c}{U_\infty} \tag{6}$$

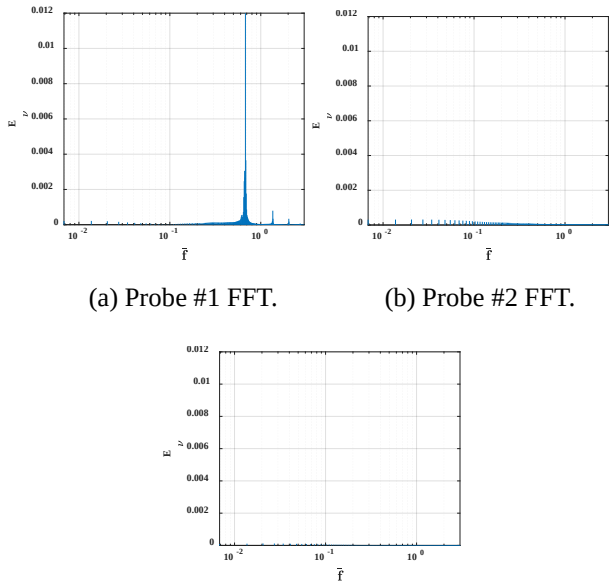

(a) Probe #1 FFT. (b) Probe #2 FFT.

(c) Probe #3 FFT.

Fig. 14: Cross-stream velocity FFT power spectra of 3 probe locations.

3.3 Active Flow Control

As previously reviewed, the airfoil boundary layer control can significantly improve its aerodynamic performance. Controlling and modifying the inherent instabilities in the boundary layer is a very effective means of flow control, and one way to achieve this is through periodic excitation[20-22].
In this simulation, periodic excitation is achieved economically (lowest energy addition/requirement) through a slat near the airfoil leading edge that periodically allows for the passing (blowing) of air from below the lower surface of the airfoil to its upper surface in an inertial manner.

Table 2: A quantitative summary of the open-loop periodic slat simulations results.

#	Simulation	Normalized Frequency ($\bar{f}$)	Control Start Time ($\bar{t}$)	ΔC_L%	$\frac{\Delta C_L}{\Delta C_D}$%
1	No slat /Clean Closed slat	–	–	0.0000	0.0000
2	Open slat No Control	–	–	7.9937	3.1030
3	AFC	0.68	0.00	4.8853	1.8851
4	AFC	0.68	36.50	6.8479	2.6530
5	AFC	6.85	0.00	-0.5013	-0.2188
6	AFC	6.85	8.76	1.3494	0.5266
7	AFC	6.85	43.50	5.8128	2.1859
8	AFC	13.69	0.00	-1.0894	-0.1206
9	AFC	13.69	43.50	5.5926	2.1416
10	AFC	136.99	36.50	5.4335	2.4385

For open-loop control, the flow was controlled by a periodic slat (Open/Closed) that was simulated using porosity model described earlier in section 2.4. Several AFC simulations were carried out for different parameters. One of which is the excitation frequency, where f, in Eq. (3) is substituted by the dominant frequencies obtained from FFT analysis in section 3.2, alongside testing other values in order to obtain the most convenient one. The other variable is time, where the different excitation initiation times had been tested. AFC was tested at different times $\boldsymbol{t}$, in Eq. (3) such as at the start of simulation ($\bar{t} = 0$), at a transient time ($\bar{t} = 8.76$), and at a complete shedding (wake formation) time ($\bar{t} = 43.50$). A summary of these trials is tabulated in Table 2.

The shown results in Fig. 15a and Fig. 15b are samples from the results in Table 2, namely case #4 which has the best improvements in the lift coefficient, drag coefficient, and the aerodynamic efficiency distribution at the dominant domain frequency $\bar{f} = 0.68$.

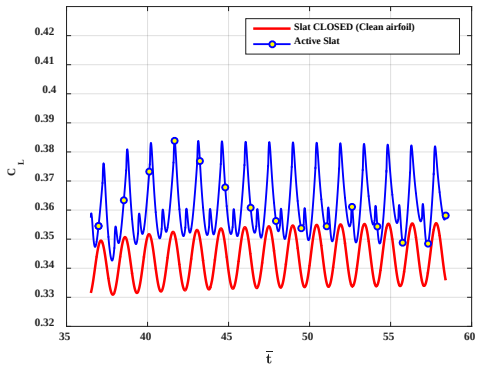

(a) Temporal variation of the Lift coefficient.

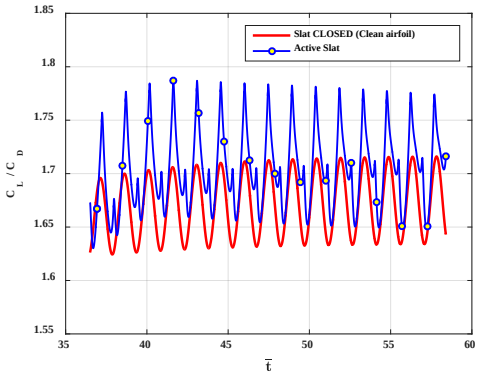

(b) Temporal variation of the aerodynamic efficiency.

Fig. 15: Aerodynamic properties temporal variation for clean/active slat with periodic porosity ($\bar{f} = 0.68$).

Additionally, Fig. 16 shows the achievement in the lift coefficient with respect to the input frequency. Whereas Fig. 17 shows that using the slat improves the mixing of the flow on the upper surface of the airfoil compared to the case of the conventional one. Consequently, the pressure drops (implying delayed flow separation) and indicating that the lift from the airfoil is increased as previously shown in Table 2.

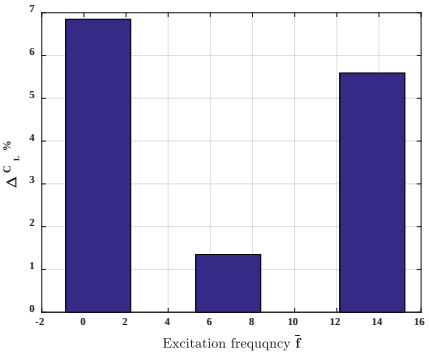

Fig. 16: Averaged lift coefficient percentage increase by AFC.

From the previous results, it is clear that starting the active slat excitation (control) after the full wake (shedding) is formed showed better aerodynamic efficiency for all tested frequencies rather than starting the excitation from the beginning of the simulation. Thus, this will save much computational time and cost. As expected from the FFT analysis, the dominant frequency showed the best results among other active control results. Likewise, the recent results obtained by Elhadidi et al.[16], the open-loop (uncontrolled) slat shows best results among all open-loop trials near the same angle of attack. Consequently, closed-loop implementation within OpenFOAM's solver is essential as a next step for achieving better aerodynamic performance.

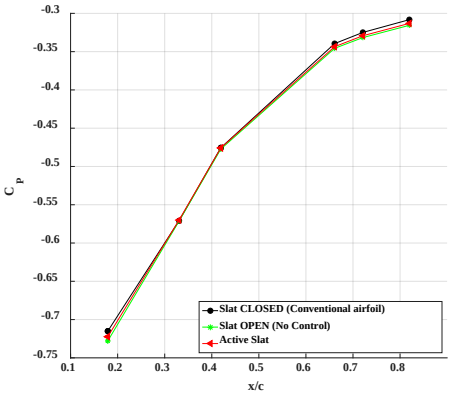

Fig. 17: Averaged pressure coefficient on the airfoil upper surface for different conditions.

4. Conclusions

The objective of this research is to investigate the influence of active flow control on the improvement of the airfoil aerodynamic properties. Thus, better aerodynamic efficiency, delayed separation, reduced drag force, and less unsteady fluctuations. To achieve this, a flow simulation around both clean and slatted configurations of a DU96-W-180 airfoil was done using OpenFOAM. Frequency analysis was done using FFT to three distinctive domain points to get the dominant frequencies.

Finally, active flow control was applied using a novel active slat operating at the dominant frequencies obtained earlier to excite the flow leading to better flow attachments and aerodynamic properties.

- The use of the slat resulted in an accelerated downstream flow, hence, increased mixing and improved performance of the airfoil.
- Frequency analysis techniques, namely FFT, had contributed well in the flow control analysis by narrowing the values of the actuation frequency. It showed the most dominant frequencies to be used in the active flow control actuation. Its vale was found to be $\overline{f} = 0.68$ and is located in the wake region. The reason behind this is that the downstream vortex shedding had high frequency and disturbed flow than upstream locations. Thus, FFT saved much computational time that would be wasted on testing a wide range of values.
- Obviously, slatting the airfoil and allowing a fresh (accelerated) boundary layer to add extra momentum to the flow improves the mixing and consequently the performance of the airfoil. An improvement in the lift coefficient was achieved of up to 8% and in the overall aerodynamic efficiency by 3% compared to the clean airfoil configuration. However, compared to the slatted uncontrolled case, the improvement was not enough promising, thus imposing a high necessity to apply closed-loop control to get better desired results.
- Active flow control simulations were applied using different actuation frequencies. It was deduced, as expected, that the dominant frequency showed the best results among all other open-loop results. The lift enhancements were up to 7% in the lift coefficient and 3% in the overall aerodynamic efficiency compared to the clean airfoil configuration.

For future work, it is recommended to investigate various slat locations to determine optimum location. Besides, applying closed loop (feedback) control is necessary to get optimized control action and yield better aerodynamic results on the airfoil. Increasing *Re* and solving for the turbulent flow need to be investigated. In addition, different angles of attacks should be studied to lock to the most critical and responsive one. Additionally, extension of this work to 3D simulations will be effective in matching practical wing cases. Furthermore, this work could be extended beyond fixed wing applications to include rotary blades. One of the promising applications is active control of the blade flutter of wind turbines using aerodynamic control[18, 23].

References

1) M. Jahanmiri, Active Flow Control: A Review, Research Report, Chalmers University of Technology, Göteborg, 12 (2010).
2) A. Gross and H. F. Fasel, CFD for Investigating Active Flow Control, AIAA 4th Flow Control Conference, Seattle, Washington (2008).
3) D. N. Miller and R. D. Joslin, *Fundamentals and Applications of Modern Flow Control*, AIAA, Reston, VA, (2009).
4) S. S. Collis, R. D. Joslin, A. Seifert, and V. Theofilis, Issues in active flow control: theory, control, simulation, and experiment, *Progress in Aerospace Sciences* **40**, Elsevier, May-July, pp. 237–289 (2004).
5) K. T. Barlas and G. V. Kuik, Review of state of the art in smart rotor control research for wind turbines, *Progress in Aerospace Sciences* **46**, 1, pp. 1–27 (2010).
6) L. N. I. Cattafesta, S. Garg, and D. Shukla, The Development of Piezoelectric Actuators for Active Flow Control, *AIAA Journal* **39**, 8, pp. 1562–1568 (2001).
7) J. Mathew, Q. Song, B. V. Sankar, M. Sheplak, and L. N. Cattafesta, Optimized Design of Piezoelectric Flap Actuators for Active Flow Control, *AIAA Journal* **44**, 12, pp. 2919–2928 (2006).
8) A. Dialoupis, Active Flow Control Using Plasma Actuators Application on Wind Turbines, Master's thesis, Delft University of Technology, (2014).
9) A. Glezer and M. Amitay, Synthetic Jets, *Annual Review of Fluid Mechanics* **34**, pp. 503–529 (2002).
10) R. Raju, R. Mittal, Q. Gallas, and L. Cattafesta, Scaling of Vorticity Flux and Entrance Length Effects in Zero-Net Mass-Flux Devices, 35th AIAA Fluid Dynamics Conference and Exhibit (2005).
11) L. N. Cattafesta, and M. Sheplak, Actuators for Active Flow Control, *Annual Review of Fluid Mechanics* **43**, 1, 247–272 (2011).
12) E. Moreau, Airflow Control by Non-Thermal Plasma Actuators, *Journal of Physics D: Applied Physics* **40**, pp. 605–636 (2007).
13) T. C. Corke, C. L. Enloe, and S. P. Wilkinson, Dielectric barrier discharge plasma actuators for flow control, *Annu. Rev. Fluid Mech.* **42**, 505–29 (2010).
14) A. M. O. Smith, High-lift aerodynamics, *Journal of Aircraft* **12**, 6, pp. 501–530 (1975).
15) T. M. Soltan, Application of Active Slat to Control Flow over a NACA 4418 airfoil at Re=40,000, Master's thesis, Cairo University (2015).
16) B. Elhadidi, I. Elqatary, O. Mohamady, and H. Othman, Experimental and Numerical Investigation of Flow Control Using a Novel Active Slat, *International Journal of Mechanical, Aerospace, Industrial, Mechatronic and Manufacturing Engineering* **9**, 1, pp. 21–25 (2015).
17) R. Raju and R. Mittal, Dynamics of Airfoil Separation Control Using Zero-Net Mass-Flux

Forcing, *AIAA Journal* **46**, 12 (2008).

18) A. M. Halawa, Active Control for Airfoil with Smart Slat, Master's thesis, Cairo University (2016).
19) OpenFOAM's Programmers/Users Guide/Official Website, http://www.openfoam.org/. Accessed: (2015).
20) F. Hsiao, C. Liu, and J.-Y. Shyu, Control of Wall-Separated Flow by Internal Acoustic Excitation, *AIAA Journal* **28**, 08, pp. 1440–1446 (1990).
21) A. Seifert, A. Darabi, and I. Wygnanski, Delay of Airfoil Stall by Periodic Excitation, *Journal of Aircraft* **33**, 4, pp. 691–698 (1996).
22) K. Zaman, A. Bar-Sever, and S. Mangalam, Effect of Acoustic Excitation on the Flow Over and Low-Re Airfoil, *Journal of Fluid Mechanics* **182**, pp. 127–148 (1987).
23) A. M. Halawa, B. Elhadidi, and S. Yoshida, POD & MLSM Application on DU96-W180 Wind Turbine Airfoil, *Evergreen*, **4**, 1, pp. 36-43 (2017).
24) M. I. El-desouky "Flow Control For Circular Cylinder Using Proper Orthogonal Decomposition". Master's thesis, Cairo University, 2009.